

# Nonlocal interaction and quantum friction in sliding $\text{Bi}_2\text{Se}_3$ topological surfaces

Feiyi Liu<sup>1,\*</sup>, Ming Guo<sup>1</sup>, Mingyang Liu<sup>1,\*\*</sup>, Ruanjing Zhang<sup>2</sup>, and Yang Wang<sup>3</sup>

<sup>1</sup>School of Physics, Electrical and Energy Engineering, Chuxiong Normal University, Chuxiong, 675000, China

<sup>2</sup>Institute of Theoretical Physics, School of Science, Henan University of Technology, Zhengzhou, 450001, China

<sup>3</sup>School of Big Data and Basic Science, Shandong Institute of Petroleum and Chemical Technology, Dongying, 257061, China

\*fyliu@cxtc.edu.cn

\*\*18788549890@163.com

## ABSTRACT

Topological insulator  $\text{Bi}_2\text{Se}_3$  thin films exhibit unique electronic properties arising from their topologically protected surface states. In a theoretical model capturing the essential physics of Dirac electrons in  $\text{Bi}_2\text{Se}_3$ , we study excitations and dissipation in two infinite parallel metallic plates undergoing relative motion. The degrees of freedom of the electrons in both plates are modeled using the 1+2 dimensional Dirac field, and a nonlocal potential is selected to describe the interaction between the two plates. The internal relative motion is introduced via a Galilean boost, with one plate assumed to slide relative to the other. We then calculate the effective action of the system and derive the vacuum occupation number in momentum space using a perturbative method. Numerical plots reveal that the vacuum occupation number, as a function of momentum, is isotropic for a motion speed  $v = 0$  and anisotropic for nonzero  $v$ . The relative motion induces energy transfer between the plates, leading to on-shell excitations in a manner analogous to the dissipative process of the Schwinger effect. Consequently, we study the motion-induced dissipation effects and the dissipative forces through the quantum action. By using experimental Fermi velocities of  $\text{Bi}_2\text{Se}_3$ , our results demonstrate that both the imaginary part of the quantum action due to the motion boost and the dissipative force exhibit a threshold as functions of  $v$ , and both are positively correlated with  $v$ .

## 1 Introduction

Topological insulators represent a novel quantum state of matter characterized by an insulating bulk and topologically protected gapless surface states<sup>1,2</sup>. Among various topological insulator materials,  $\text{Bi}_2\text{Se}_3$  has emerged as an ideal platform due to its relatively large bulk band gap and simple surface electronic structure<sup>3,4</sup>. Particularly in the thin-film limit,  $\text{Bi}_2\text{Se}_3$  exhibits remarkable tunability of its topological surface states: surface state hybridization opens a tunable gap at the Dirac point<sup>5</sup>, surface engineering enables optimization of Dirac cone isolation<sup>6</sup>, and strain can modulate the bulk gap and even induce topological phase transitions<sup>7</sup>. These highly controllable topological interface states provide a unique platform for investigating fundamental physical processes in low-dimensional quantum systems, especially in exploring quantum dissipation mechanisms induced by relative motion, which is of paramount importance for understanding energy transfer in nanoscale devices.

The study of open quantum systems (OQS) has gained significant attention over the decades in the field of condensed matter physics<sup>8</sup>. An important feature of OQSs is dissipation and its related dynamics that arise when the systems are coupled with environments. For such OQSs, one can partially trace over the degrees of freedom (DOFs) of the environments to obtain the effective dynamics of the system<sup>9–13</sup>. This is similar to the process occurring in models of effective field theory, where one can obtain the effective action by integrating over some irrelevant DOFs<sup>14–18</sup>. However, there exists special cases of OQSs that do not obviously couple to environments. For instance, consider two parallel plates placed close together, where the internal DOFs of the plates couple with each other via some effective potentials. An external force acts on one of the plates to keep them moving uniformly, and this relative motion induces dissipation

and a frictional force within the plates<sup>19</sup>.

Dissipation refers to the irreversible transfer of energy. In other words, energy is carried by particles or quasi-particles<sup>20</sup>. For instance, in the dynamical Casimir effect involving two metal plates separated by a vacuum gap, on-shell photons are excited in the vacuum gap between the plates<sup>21</sup>. If the relative speed between the two plates is small, on-shell photons cannot be excited; however, the internal DOFs within the plates are still excited<sup>22</sup>. Another example in condensed matter physics is that two insulated plates stick together and slide relative to each other, causing phonons at the interfaces to be excited due to the sliding contact<sup>23</sup>. The quantum spins in the two plates interact with each other through magnetic exchange or dipole coupling, and this interaction causes the relative motion to excite magnons in the plates, also representing this type of energy transfer<sup>24</sup>. Electronic friction is also a prime example, in this case two metal plates stick together and move relative to each other, with the electrons in each plate interacting through direct exchange coupling<sup>25,26</sup>. The models discussed above are all semiclassical and do not strictly account for quantum effects.

In a detailed discussion of OQSs, the influence of quantum effects on microscopic systems cannot be ignored, especially the dissipation described by the quantum action. A functional approach has been tried to study the quantum effective dynamics of moving, planar, dispersive mirrors and etc, in different numbers of dimensions<sup>27</sup>. Viotti *et al* studied the dissipative effects and decoherence induced on a particle moving at constant speed in front of a dielectric plate in quantum vacuum, using a Closed-Time-Path (CTP) integral formulation to account for finite-temperature corrections<sup>28</sup>. Farias *et al* discussed the Casimir friction phenomenon in a system consisting of two flat, infinite, and parallel graphene sheets coupled to the vacuum electromagnetic (EM) field<sup>29</sup>. The dissipation and decoherence of the particle's internal DOFs were studied with regard to a particle moving in front of a dielectric plate.<sup>30</sup> In previous work, we focused on the quantum motion-driven dissipation effect in a plasmon-magnon coupling system, and calculated the plasmon production probability and the sliding frictional force in the system<sup>31</sup>. These studies attempt to explain quantum effects, especially dissipation, in OQSs from various perspectives, which has inspired our work.

In this paper, we study the quantum excitations and dissipation of two infinite parallel metallic plates moving relative to each other along their interface. This system is similar to the 3D topological insulator  $\text{Bi}_2\text{Se}_3$ <sup>3,32</sup>. Massive Dirac electrons are considered in this model and a nonlocal Anderson mixed coupling is introduced to transmit friction, instead of relying on vacuum fluctuations of the electromagnetic field. We assume a relative sliding is driven by an external field for excitations and dissipation, and analyze the interaction of electrons in the two plates via a nonlocal potential. To study the excitations, we start with the DOFs associated with each plate using massive Dirac fermions and write the effective action of the electrons by considering one plate sliding relative to the other. By focusing on the time evolution of the system, we calculate the probability of particle production and derive the vacuum occupation number of the fixed plate perturbatively. Since the process of relative motion inducing on-shell excitations is very similar to the Schwinger effect, we can study the quantum effects of this process through the method of path integrals, and then obtain the imaginary part of the quantum action and the dissipative force, with real experimental Fermi velocity  $v_F$ .

The main structure of this paper is as follows. In Section 2, we introduce the electronic structures and topological properties of  $\text{Bi}_2\text{Se}_3$  that motivate our theoretical framework. In Section 3, the microscopic model will be given. Section 4 discuss the time evolution of the system and calculate the probability of particle production. In Section 5, we focus on the excitations of the system. Section 6 is about quantum effects and dissipation. Section 7 is the conclusion of this work.

## 2 Electronic structures and topological properties of three-dimensional and two-dimensional $\text{Bi}_2\text{Se}_3$

The theoretical model developed in this study investigates motion-induced dissipation between two parallel plates described by massive Dirac fermions. The model is motivated by the distinctive electronic properties of  $\text{Bi}_2\text{Se}_3$ <sup>3,32</sup>, which band structure is given in Figure 1. The low-energy excitations on the surface of  $\text{Bi}_2\text{Se}_3$  are governed by massless Dirac fermions that exhibit spin-momentum locking, a fundamental feature incorporated into the Hamiltonian of our model. Consequently, understanding the electronic structure of  $\text{Bi}_2\text{Se}_3$  in both its three-dimensional bulk form and its two-dimensional thin-film limit is essential for establishing the theoretical framework of this work.

Bismuth selenide ( $\text{Bi}_2\text{Se}_3$ ) crystallizes in a rhombohedral structure with space group  $R\bar{3}m$  (No. 166). The crystal can be conveniently described as a stack of quintuple layers (QLs) along the trigonal  $c$  axis, where each QL consists of atomic planes arranged in the sequence Se(1)-Bi-Se(2)-Bi-Se(1). The bonding within each QL is predominantly covalent-ionic, whereas adjacent QLs are held together by weak van der Waals interactions. This layered configuration

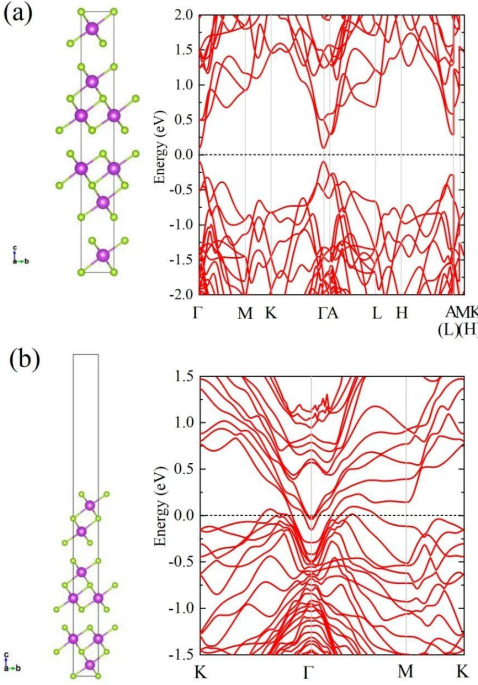


**Figure 1.** The band structure of  $\text{Bi}_2\text{Se}_3$  in (a) three-dimension and (b) two-dimension.

forms the structural basis for thin-film exfoliation and epitaxial growth<sup>5,6</sup>. As a direct consequence of the bulk topology, the material hosts robust, gapless metallic surface states that can be described by a massless Dirac Hamiltonian. These surface states form a Dirac cone with a linear energy dispersion  $E(k) = \pm \hbar v_F |\mathbf{k}|$ , where  $v_F$  denotes the Fermi velocity. The electron spin is oriented perpendicular to its momentum, a phenomenon known as spin-momentum locking, which suppresses backscattering from nonmagnetic impurities and preserves the topological protection of the surface states<sup>5,7</sup>.

When the thickness of  $\text{Bi}_2\text{Se}_3$  is reduced to the nanometer scale, typically below about six quintuple layers, a tunable dimension arises due to quantum confinement and intersurface coupling. In this quasi-two-dimensional configuration, the topological surface states from the top and bottom surfaces, which are independent in thick crystals, begin to hybridize. This hybridization opens an energy gap  $\Delta_f$  at the Dirac point<sup>5</sup>. The magnitude of this gap is highly sensitive to the film thickness  $d$ , offering an effective means to tailor the electronic structure. This tunable energy gap plays a central role in the present model, as it directly influences the density of low-energy states and the phase space available for excitations. The Dirac cone of  $\text{Bi}_2\text{Se}_3$  can be effectively tuned through surface engineering, such as oxygen substitution on surface Se sites, which modifies the surface potential and isolates the Dirac cone within the bulk band gap, thereby enhancing topological transport<sup>6</sup>. In addition, the electronic structure is highly sensitive to external strain, where uniaxial compression can alter the bulk band gap and even induce a topological phase transition by modifying spin-orbit coupling and Coulombic interactions<sup>7</sup>.

In this study, the essential physics of two coupled  $\text{Bi}_2\text{Se}_3$  surfaces is modeled by two parallel slabs whose internal degrees of freedom are described by a (2+1)-dimensional massive Dirac field. The massive Dirac Hamiltonian used in our analysis (Eq. (3)) directly corresponds to the effective Hamiltonian of  $\text{Bi}_2\text{Se}_3$  surface states. The nonlocal interaction potential  $U(x, y)$  between the slabs (Eq. (5)) represents the intersurface hybridization in  $\text{Bi}_2\text{Se}_3$  films, or more generally, the coupling between two low-dimensional Dirac systems. The relative motion of the slabs introduces a Galilean acceleration, creating a nonequilibrium state analogous to that between two topological insulator surfaces. The relative velocity  $v$  serves as a tuning parameter, similar to strain, thickness, or chemical substitution that modify the properties of real two-dimensional  $\text{Bi}_2\text{Se}_3$  structures. The anisotropy of the vacuum occupation number  $n_L(\mathbf{k})$  caused



**Figure 2.** Schematic picture of the system.

by a nonzero  $v$  (Section 5) and the resulting quantum dissipation (Section 6) can be experimentally probed through sliding interfaces or nonequilibrium transport in topological insulator films and heterostructures. The tunable electronic structure of both three-dimensional and two-dimensional  $\text{Bi}_2\text{Se}_3$  therefore provides a robust physical foundation and a promising materials platform for studying the quantum dissipation phenomena discussed in this work.

### 3 The microscopic model

The model of  $\text{Bi}_2\text{Se}_3$  system we consider in this study is the interface between two infinite metallic plates, which is shown in Fig. 2. For easy identification, one plate is marked as L-plate and the other as R-plate. Since our purpose is to study motion driven excitations and dissipation, relative sliding is required in the system. Here we assume that the L-plate is at rest in the laboratory frame, and the R-plate is moving along the interface. The total area of each plate is  $V$ , and the total evolution time for fiction of the system is  $T$ . To analyze the model, a 1+3 dimensional space-time coordinate system is constructed as  $X = (x^0, x^1, x^2, x^3)^\top$ , where  $x^0 = ct$  is the time coordinate with the speed of light  $c$  and  $\{x^1, x^2, x^3\}$  are the Cartesian coordinates. The axis of  $x^3$  is set to be perpendicular to the L-plate. The space-time coordinates for the 1+2 dimensional space-time domain of the L-plate read  $x = (x^0, x^1, x^2)^\top$  and the spacial components are written as  $x = (x^1, x^2)^\top$ . We follow the convention of natural unit such that  $\hbar = c = 1$ . The corresponding covariant components of a space time vector is  $k_\mu = \eta_{\mu\nu} k^\nu$ , i.e.  $k_0 = k^0$ ,  $k_1 = -k^1$  and  $k_2 = -k^2$ , where  $\eta_{\mu\nu} = \text{diag}(1, -1, -1, -1)$  is the Minkovski metric. So the inner product of two space time vectors is  $k \cdot x = k^0 x^0 - \mathbf{k} \cdot \mathbf{x}$ .

To study the excitations of large numbers of materials, we start from the DOFs living on each plates via the 1+3 dimensional massive Dirac fermions, which can be defined as:

$$\psi_{R/L}(x) = (c_{R/L\uparrow}(x), c_{R/L\downarrow}(x))^\top, \quad (1)$$

$$\psi_{R/L}^\dagger(x) = (c_{R/L\uparrow}^\dagger(x), c_{R/L\downarrow}^\dagger(x)). \quad (2)$$

Here  $c_{R/L\uparrow}^\dagger(x)$  and  $c_{R/L\downarrow}^\dagger(x)$  represent the components of the Dirac spinor, since surface states of both topological insulators are fermions. The free parts of the action corresponding to the free Dirac fermions on the two plates of our system can be expressed as<sup>33</sup>:

$$S^0 = \int d^3x \psi_L^\dagger [i\partial_0 - v_F \sigma^1 (-i\partial_1) - v_F \sigma^2 (-i\partial_2) - \sigma^3 v_F m] \psi_L + \int d^3x \psi_R^\dagger [i\partial_0 - v_F \sigma^1 (-i\partial_1) - v_F \sigma^2 (-i\partial_2) - \sigma^3 v_F m] \psi_R. \quad (3)$$

The upper term describes the free action of the electrons living on the surface of L-plate, and the second line is for the R-plate. The integral measure refers to  $\int d^3x' = \int_{-T/2}^{T/2} dx^0 \int_{-\infty}^{\infty} dx^1 \int_{-\infty}^{\infty} dx^2$ .  $v_F$  is the Fermi velocity of the fermions, and  $\sigma$  is the Pauli matrix as:

$$\sigma^1 = \begin{pmatrix} 0 & 1 \\ 1 & 0 \end{pmatrix}, \sigma^2 = \begin{pmatrix} 0 & -i \\ i & 0 \end{pmatrix}, \sigma^3 = \begin{pmatrix} 1 & 0 \\ 0 & -1 \end{pmatrix}. \quad (4)$$

Usually, real experiments take into account the influence of an external magnetic field, which causes the system to exhibit spin-orbit coupling, resulting in a mass term in the action. For example, an uniform applied magnetic field  $\mathbf{B} = (0, 0, v_{\text{FM}})^T$  is directed along the  $x^3$  axis.

In this study of  $\text{Bi}_2\text{Se}_3$  model, electrons on the two plates are considered to couple via a direct-exchange interaction, similar to the Anderson mixed model<sup>34</sup>. It involves local interactions and the electron-electron interaction typically involves direct exchange, ignoring nonlocal electron exchange coupling. However, the interaction occurs between two many-electron systems with nonlocal coupling, it should include not only a direct exchange term but also a nonlocal term. By taking a real-valued nonlocal potential  $U(x, y) = U(x^0, \mathbf{x}; y^0, \mathbf{y})$ , this nonlocal Anderson mixed model where the fermions belonging to the two plates interact with each other can be written as:

$$S^{\text{int}} = g \int d^3x \int d^3y [\psi_L^\dagger(x) U(x, y) \psi_R(y) + h.c.]. \quad (5)$$

Here  $g$  is constant of small coupling, and  $h.c.$  means the hermite conjugate of the term  $\psi_L^\dagger(x) U(x, y) \psi_R(y)$ . Since the nonlocal potential  $U$  indicates the interaction propagates at a finite speed and the Anderson mixed coupling is used to describe quantum electrodynamics (QED), the most natural expression for  $U$  is the Feynman propagator of a massless particle, i.e., a Green's function with poles  $k^0 = \pm|\mathbf{k}|$ , as:

$$U(x^0, \mathbf{x}; y^0, \mathbf{y}) = \int \frac{d^3k}{(2\pi)^3} \frac{\exp[ik^0(x^0 - y^0) - i\mathbf{k} \cdot (\mathbf{x} - \mathbf{y})]}{\sqrt{(k^0)^2 - \mathbf{k}^2 + i\epsilon}}. \quad (6)$$

The integral measure in the momentum space refers to  $\int \frac{d^3k}{(2\pi)^3} = \int_{-\infty}^{\infty} \frac{dk^0}{2\pi} \int_{-\infty}^{\infty} \frac{dk^1}{2\pi} \int_{-\infty}^{\infty} \frac{dk^2}{2\pi}$ . By introducing the (1+2) dimensional Fourier momentum  $k = (k^0, k^1, k^2)^T$ , the spacial components can be written as  $\mathbf{k} = (k^1, k^2)^T$ . In Eq. (6), it obviously has two singular point on the  $k^0$  complex plane, which means  $U$  can be regarded as a propagator of massless particles.

Now, we can obtain the total action of the system as:

$$\begin{aligned} S &= S^0 + S^{\text{int}} \\ &= \int d^3x \psi_L^\dagger [i\partial_0 - v_F \sigma^1(-i\partial_1) - v_F \sigma^2(-i\partial_2) - \sigma^3 v_{\text{FM}}] \psi_L \\ &\quad + \int d^3x \psi_R^\dagger [i\partial_0 - v_F \sigma^1(-i\partial_1) - v_F \sigma^2(-i\partial_2) - \sigma^3 v_{\text{FM}}] \psi_R \\ &\quad + g \int d^3x \int d^3y [\psi_L^\dagger(x) U(x, y) \psi_R(y) + h.c.]. \end{aligned} \quad (7)$$

Since our goal is to study motion-dependent dissipation, for simplicity, we assume that the L-plate is at rest in the laboratory frame, while the R-plate moves at a constant velocity,  $\mathbf{v} = (0, v)^T$ , along the  $x^1$ -axis due to an external force. This movement results in a Galilean boost acting on the R-plate along the  $x^1$  axis:

$$\begin{pmatrix} x'^0 \\ x'^1 \\ x'^2 \end{pmatrix} = \begin{pmatrix} 1 & 0 & 0 \\ -v & 1 & 0 \\ 0 & 0 & 1 \end{pmatrix} \begin{pmatrix} x^0 \\ x^1 \\ x^2 \end{pmatrix}. \quad (8)$$

Thus, the total action becomes:

$$\begin{aligned} S &= S^0 + S^{\text{int}} \\ &= \int d^3x \psi_L^\dagger [i\partial_0 - v_F \sigma^1(-i\partial_1) - v_F \sigma^2(-i\partial_2) - \sigma^3 v_{\text{FM}}] \psi_L \\ &\quad + \int d^3x \psi_R^\dagger [i\partial_0 + v(i\partial_1) - v_F \sigma^1(-i\partial_1) - v_F \sigma^2(-i\partial_2) - \sigma^3 v_{\text{FM}}] \psi_R \\ &\quad + g \int d^3x \int d^3y [\psi_L^\dagger(x) U(x, y) \psi_R(y) + h.c.]. \end{aligned} \quad (9)$$

By the Fourier transformations  $\psi_R(x) = \int \frac{d^3k}{(2\pi)^3} \psi_R(k) \exp(ik \cdot x)$  and  $\psi_L(x) = \int \frac{d^3k}{(2\pi)^3} \psi_L(k) \exp(ik \cdot x)$ , we can achieve the total action in momentum space, expressed as:

$$\begin{aligned}
S &\equiv S[\psi_R, \psi_L] = S^0 + S^{\text{int}} \\
&= \int \frac{d^3k}{(2\pi)^3} \psi_L^\dagger(k) [k^0 + v_F \sigma^1 k^1 + v_F \sigma^2 k^2 - \sigma^3 v_F m] \psi_L(k) \\
&\quad + \int \frac{d^3k}{(2\pi)^3} \psi_R^\dagger(k) [k^0 - v_F k^1 + v_F \sigma^1 k^1 + v_F \sigma^2 k^2 - \sigma^3 v_F m] \psi_R(k) \\
&\quad + g \int \frac{d^3k}{(2\pi)^3} \left[ \frac{\psi_L^\dagger(k) \psi_R(k)}{\sqrt{k^\mu k_\mu + i\epsilon}} + h.c. \right] \\
&= \int \frac{d^3k}{(2\pi)^3} \begin{pmatrix} c_{L\uparrow}^\dagger(k) & c_{L\downarrow}^\dagger(k) \end{pmatrix} \begin{pmatrix} k^0 - v_F m & v_F(k^1 - ik^2) \\ v_F(k^1 + ik^2) & k^0 + v_F m \end{pmatrix} \begin{pmatrix} c_{L\uparrow}(k) \\ c_{L\downarrow}(k) \end{pmatrix} \\
&\quad + \int \frac{d^3k}{(2\pi)^3} \begin{pmatrix} c_{R\uparrow}^\dagger(k) & c_{R\downarrow}^\dagger(k) \end{pmatrix} \begin{pmatrix} k^0 - v_F k^1 - v_F m & v_F(k^1 - ik^2) \\ v_F(k^1 + ik^2) & k^0 - v_F k^1 + v_F m \end{pmatrix} \begin{pmatrix} c_{R\uparrow}(k) \\ c_{R\downarrow}(k) \end{pmatrix} \\
&\quad + g \int \frac{d^3k}{(2\pi)^3} \left[ \frac{1}{\sqrt{k^\mu k_\mu + i\epsilon}} \begin{pmatrix} c_{L\uparrow}^\dagger(k) & c_{L\downarrow}^\dagger(k) \end{pmatrix} \begin{pmatrix} c_{R\uparrow}(k) \\ c_{R\downarrow}(k) \end{pmatrix} + h.c. \right], \tag{10}
\end{aligned}$$

which is one of the key points to calculate the dissipation effect induced by relative motion in our model.

## 4 Time evolution and particle production

Next, we focus on the time evolution of the system. In general, the time evolution can be considered adiabatic, meaning that if the system is isolated ( $v = 0$ ), it would always return to the initial vacuum state after a total evolution time  $T$ . To describe the interaction adiabatically, we set the initial state of the system expressed in Dirac notation as the free vacuum state  $|i\rangle = |0\rangle$  at time  $-\frac{T}{2}$ , and satisfying orthogonality  $\langle 0|0\rangle = 1$ <sup>35</sup>. Thus, the final state  $|f\rangle$  can be written as:

$$|f\rangle = |f_0\rangle = \mathcal{U}_I\left(\frac{T}{2}, -\frac{T}{2}\right)|0\rangle = |0\rangle \exp(i\Gamma_0), \tag{11}$$

where  $\Gamma_0$  is a real valued object and  $\mathcal{U}_I\left(\frac{T}{2}, -\frac{T}{2}\right)$  is the time evolution operator in interaction picture<sup>36</sup>. The overlap between initial and final state reads:

$$\langle i|f_0\rangle = \langle 0|\mathcal{U}_I\left(\frac{T}{2}, -\frac{T}{2}\right)|0\rangle = \langle 0|0\rangle \exp(i\Gamma_0) = \exp(i\Gamma_0). \tag{12}$$

In an open system where an external force acts on the R-plate to maintain relative motion, the system's state cannot obviously return to the initial vacuum state at the end. Instead, the final state should include all possible states, meaning that  $\Gamma$  is not real-valued, resulting in an unstable vacuum. To tell the detailed story, we define the eigenstate of the system's free Hamiltonian as  $|n\rangle$ , with the complete set of states:

$$\sum_n |n\rangle \langle n| = \mathbb{I}. \tag{13}$$

Then, the normalization of the final state can be expressed as:

$$\begin{aligned}
\langle f|f\rangle &= \langle 0|\mathcal{U}_I^\dagger\left(\frac{T}{2}, -\frac{T}{2}\right)\mathcal{U}_I\left(\frac{T}{2}, -\frac{T}{2}\right)|0\rangle \\
&= \sum_n \langle 0|\mathcal{U}_I^\dagger\left(\frac{T}{2}, -\frac{T}{2}\right)|n\rangle \langle n|\mathcal{U}_I\left(\frac{T}{2}, -\frac{T}{2}\right)|0\rangle \\
&= \langle 0|\mathcal{U}_I^\dagger\left(\frac{T}{2}, -\frac{T}{2}\right)|0\rangle \langle 0|\mathcal{U}_I\left(\frac{T}{2}, -\frac{T}{2}\right)|0\rangle + \sum_{n>0} \langle 0|\mathcal{U}_I^\dagger\left(\frac{T}{2}, -\frac{T}{2}\right)|n\rangle \langle n|\mathcal{U}_I\left(\frac{T}{2}, -\frac{T}{2}\right)|0\rangle \\
&= 1. \tag{14}
\end{aligned}$$

The terms for  $n > 0$  refer to the probability of particle production (the bound states are omitted for simplicity), so  $\langle 0 | \mathcal{U}_1^\dagger(\frac{T}{2}, -\frac{T}{2}) | 0 \rangle \langle 0 | \mathcal{U}_1(\frac{T}{2}, -\frac{T}{2}) | 0 \rangle$  is regarded as the transition probability from vacuum to vacuum, i.e. the vacuum persistence probability<sup>8</sup>. And the corresponding amplitude  $Z = \langle 0 | \mathcal{U}_1(\frac{T}{2}, -\frac{T}{2}) | 0 \rangle = e^{i\Gamma}$  is called Vacuum Persistence Amplitude(VPA). Thus, the probability of particle production can be written as:

$$\begin{aligned} \mathcal{P} &= 1 - \langle 0 | \mathcal{U}_1^\dagger(\frac{T}{2}, -\frac{T}{2}) | 0 \rangle \langle 0 | \mathcal{U}_1(\frac{T}{2}, -\frac{T}{2}) | 0 \rangle \\ &= 1 - \exp(-i\Gamma^*) \exp(i\Gamma) \\ &= 1 - \exp(-2i\text{Im}\Gamma), \end{aligned} \quad (15)$$

and the relative motion induces particle production in the system, which means it has on-shell excitations in both the L- and the R-plate. Now, the final state can be expressed as:

$$|f\rangle = |0\rangle \langle 0 | \mathcal{U}_1(\frac{T}{2}, -\frac{T}{2}) | 0 \rangle + \sum_{n>0} |n\rangle \langle n | \mathcal{U}_1(\frac{T}{2}, -\frac{T}{2}) | 0 \rangle, \quad (16)$$

and the final vacuum state can be written as:

$$|\Omega\rangle = |0\rangle \exp(i\text{Re}\Gamma) \exp(-i\text{Im}\Gamma), \quad (17)$$

which is different from the initial vacuum. And here the factor  $\exp(-i\text{Im}\Gamma)$  changes the modulus square of  $|\Omega\rangle$ .

In this work, we consider only the case where the final state is not far from the initial state, which can be analyzed using perturbative methods. This implies that the terms with  $n > 0$  in the final state should be small enough. In addition, the interaction within the system leads to a finite lifetime of the excitations, resulting in the system reaching a non-equilibrium steady state (NESS). Furthermore, the external force acting on the R-plate excites particles in the system, and, due to the interaction, the particles decay. These two processes occur simultaneously, leading the system to reach mechanical equilibrium.

Generally, the VPA is expressed in Heisenberg picture via asymptotic states<sup>35</sup>. So firstly we define the asymptotic vacuum states  $|\text{VAC, in}\rangle$  and  $|\text{VAC, out}\rangle$  as:

$$|\text{VAC, in}\rangle = \mathcal{U}_1(0, -\frac{T}{2}) | 0 \rangle, \quad (18)$$

$$|\text{VAC, out}\rangle = \mathcal{U}_1^\dagger(\frac{T}{2}, 0) | 0 \rangle, \quad (19)$$

and then the VPA can be written as:

$$Z = \langle \text{VAC, out} | \text{VAC, in} \rangle = e^{i\Gamma}. \quad (20)$$

The vacuum expectation value of an operator  $\mathcal{O}_H$  in Heisenberg picture can be expressed as:

$$\langle \text{VAC, in} | \mathcal{O}_H | \text{VAC, in} \rangle = \frac{\langle \text{VAC, out} | \mathcal{O}_H | \text{VAC, in} \rangle}{\langle \text{VAC, out} | \text{VAC, in} \rangle}. \quad (21)$$

Here we neglect the contribution from the excited states with  $n > 0$  in Eq. (15), since we are only focusing on the NESS case that is near the initial vacuum state.

## 5 Excitations of L-plate

In the previous section, the formal equation of motion-induced particle production was given. Now, we focus on the vacuum occupation number in momentum space, including quantum effects. The relative motion induces on-shell excitations in both the L-plate and the R-plate. Here, we consider only the L-plate, but the impact of the R-plate cannot be disregarded. To obtain the effective action of the L-electrons under the influence of the R-plate, we integrate out the R-electrons in the path integral formulation of the system as<sup>36</sup>:

$$\exp(iS_{\text{eff}}[\psi_L, \psi_L^\dagger]) = \int D\psi_R D\psi_R^\dagger \exp(iS), \quad (22)$$

and then the effective action of L-electrons can be written as:

$$S_{\text{eff}}[\psi_L, \psi_L^\dagger] = \int \frac{d^3k}{(2\pi)^3} \begin{pmatrix} c_{L\uparrow}(k) \\ c_{L\downarrow}(k) \end{pmatrix}^\dagger \begin{pmatrix} k^0 - v_F m & v_F(k^1 - ik^2) \\ v_F(k^1 + ik^2) & k^0 + v_F m \end{pmatrix} \begin{pmatrix} c_{L\uparrow}(k) \\ c_{L\downarrow}(k) \end{pmatrix} + g^2 \int \frac{d^3k}{(2\pi)^3} \left[ \frac{1}{k^\mu k_\mu + i\epsilon} \begin{pmatrix} c_{L\uparrow}(k) \\ c_{L\downarrow}(k) \end{pmatrix}^\dagger \begin{pmatrix} k^0 - v_F k^1 - v_F m & v_F(k^1 - ik^2) \\ v_F(k^1 + ik^2) & k^0 - v_F k^1 + v_F m \end{pmatrix}^{-1} \begin{pmatrix} c_{L\uparrow}(k) \\ c_{L\downarrow}(k) \end{pmatrix} \right]. \quad (23)$$

To derive the vacuum occupation number of the system in momentum space perturbatively, we start with the particle number density operator, defined as:

$$\hat{n}_L(x^0, \mathbf{x}) := \psi_L^\dagger(x^0, \mathbf{x}) \psi_L(x^0, \mathbf{x}). \quad (24)$$

So the vacuum expectation value can be written as:

$$\begin{aligned} n_L(x^0, \mathbf{x}) &:= \langle \text{VAC, in} | \psi_L^\dagger(x^0, \mathbf{x}) \psi_L(x^0, \mathbf{x}) | \text{VAC, in} \rangle \\ &= \lim_{y \rightarrow x} \text{tr} \langle \text{VAC, in} | \mathcal{T}[\psi_L(x^0, \mathbf{x}) \psi_L^\dagger(y^0, \mathbf{y})] | \text{VAC, in} \rangle \\ &= \lim_{y \rightarrow x} \frac{\text{tr} \langle \text{VAC, out} | \mathcal{T}[\psi_L(x^0, \mathbf{x}) \psi_L^\dagger(y^0, \mathbf{y})] | \text{VAC, in} \rangle}{\langle \text{VAC, out} | \text{VAC, in} \rangle} \\ &= -i \lim_{y \rightarrow x} \text{tr} \Delta_L(x, y). \end{aligned} \quad (25)$$

Here ‘tr’ means tracing over the spin indices, and  $\mathcal{T}$  is the time-ordered operator.  $\Delta_L(k^0, \mathbf{k})$  is the exact propagator of the L-electrons.

Since the state of the system is a non-equilibrium steady state (NESS) and homogeneous, the exact propagator in momentum space does not depend on  $\frac{x+y}{2}$ . This means that the Fourier transform can be directly applied, as follows:

$$n_L(x^0, \mathbf{x}) = -i \lim_{y \rightarrow x} \int \frac{dk^0}{2\pi} \int \frac{d^2k}{(2\pi)^2} \text{tr}[\Delta_L(k^0, \mathbf{k})] \exp(-ik \cdot (x - y)). \quad (26)$$

After performing the  $k^0$ -integration, the corresponding expression for the vacuum occupation number in momentum space is given by:

$$n_L(\mathbf{k}) = -i \int \frac{dk^0}{2\pi} \text{tr}[\Delta_L(k^0, \mathbf{k})]. \quad (27)$$

We calculate the propagator  $\Delta_L(k^0, \mathbf{k})$  perturbatively up to order  $o(g^2)$ , and the result is:

$$\Delta_L(k^0, \mathbf{k}) = G_L(k^0, \mathbf{k}) + \frac{g^2}{k^\mu k_\mu + i\epsilon} G_L(k^0, \mathbf{k}) G_R(k^0 - v_F k^1, \mathbf{k}) G_L(k^0, \mathbf{k}). \quad (28)$$

The first term in Eq. (28) comes from the free L-electrons, specifically a loop propagator, corresponding to the contribution of vacuum energy. In the canonical approach, this loop propagator can be removed by the normal ordering of the field operators, which means the vacuum occupation number of L-electrons is zero in the free theory. The second term in Eq. (28) refers to the interaction with the R-electrons. In our study, the L-electrons evolve under an effective potential due to the integration of the R-electrons, so they can be considered as an OQS. Therefore, the vacuum occupation number of L-electrons is modified by the effective potential, meaning it is nonzero due to the interaction.

Through path integral formulas, the free electron propagators  $G_{R/L}(x)$  can be defined as<sup>36</sup>:

$$G_{R/L}(x) = \frac{\int D\psi_{R/L} D\psi_{R/L}^\dagger \exp[iS^0] \psi_{R/L} \psi_{R/L}^\dagger}{\int D\psi_{R/L} D\psi_{R/L}^\dagger \exp[iS^0]}. \quad (29)$$

The explicit expressions of L- and R- plates in momentum space can be written as:

$$G_L(k) = \frac{1}{(k^0)^2 - v_F^2(k^1)^2 - v_F^2(k^2)^2 - v_F^2 m^2 + i\epsilon} \begin{pmatrix} k^0 + v_F m & -v_F(k^1 - ik^2) \\ -v_F(k^1 + ik^2) & k^0 - v_F m \end{pmatrix}, \quad (30)$$

and

$$\begin{aligned} \tilde{G}_R(k^0, k^1, k^2) &= G_R(k^0 - vk^1, k^1, k^2) \\ &= \frac{1}{(k^0 - vk^1)^2 - v_F^2(k^1)^2 - v_F^2(k^2)^2 - v_F^2 m^2 + i\epsilon} \begin{pmatrix} k^0 - vk^1 + v_F m & -v_F(k^1 - ik^2) \\ -v_F(k^1 + ik^2) & k^0 - vk^1 - v_F m \end{pmatrix}. \end{aligned} \quad (31)$$

The relative motion causes the speed to appear in the propagator, which leads to a change in the modified vacuum occupation number. To focus on the effects of relative motion, we redefine the vacuum occupation number as:

$$\begin{aligned} n_L(\mathbf{k}) &:= -i \int \frac{dk^0}{2\pi} \text{tr}[\Delta_L(k^0, \mathbf{k}) - G_L(k^0, \mathbf{k})] \\ &= -i \int \frac{dk^0}{2\pi} \frac{g^2}{k^\mu k_\mu + i\epsilon} \text{tr}[G_L(k^0, \mathbf{k}) G_R(k^0 - vk^1, \mathbf{k}) G_L(k^0, \mathbf{k})] \\ &= 2ig^2 \int \frac{dk^0}{2\pi} \frac{1}{(k^\mu k_\mu + i\epsilon)[(k^0)^2 - v_F^2(\mathbf{k}^2 + m^2) + i\epsilon]^2 [(k^0 - vk^1)^2 - v_F^2(\mathbf{k}^2 + m^2) + i\epsilon]}. \end{aligned} \quad (32)$$

The integrand has three simple poles in the  $k^0$ -plane. Since in this study only the effects induced by the relative motion are considered, we focus on the simple poles that depend on the relative velocity  $\mathbf{v} = (v, 0)^T$ , i.e.,  $\Lambda_\pm = vk^1 \pm v_F \sqrt{(k^1)^2 + (k^2)^2 + m^2 - i\epsilon} \approx vk^1 \pm v_F \sqrt{(k^1)^2 + (k^2)^2 + m^2} \mp i\epsilon$ . The reasonable contours can be built to evaluate the integral over  $k^0$  using the residue theorem as<sup>36</sup>:

$$n_L(\mathbf{k}) = \frac{g^2 \pi (vk^1 + 2\omega_k)}{[(vk^1 + \omega_k)^2 - \mathbf{k}^2](vk^1)} + \frac{g^2 \pi (vk^1 - 2\omega_k)}{[(vk^1 - \omega_k)^2 - \mathbf{k}^2](vk^1)}, \quad (33)$$

where  $\omega_k := v_F \sqrt{\mathbf{k}^2 + m^2}$  is the dispersion of free electrons.

As a function of momentum,  $n_L(\mathbf{k})$  is isotropic for  $v = 0$ , but becomes anisotropic for nonzero  $v$ . Moreover,  $n_L(\mathbf{k})$  is time-independent, indicating that our approximation applies to a NESS regime where the system remains close to the initial vacuum state. The nonzero vacuum occupation number in momentum space shows that the interaction modifies the free vacuum, and the relative motion induces on-shell excitations from the vacuum.

## 6 Quantum dissipation

In Section 4, we discussed how relative motion induces on-shell excitations. This process is analogous to the Schwinger effect, as particle production is a dissipative process where the energy of the excitations originates from the external force<sup>37</sup>. The energy transfer within the system implies the existence of dissipative forces between the two plates. Consequently, in this section, we investigate the motion-induced dissipation effects and the corresponding dissipative forces.

From Eq. (20), the VPA can be expressed via path integral as<sup>38</sup>:

$$Z = e^{i\Gamma} = \int D\psi_R D\psi_R^\dagger \int D\psi_L D\psi_L^\dagger \exp(iS). \quad (34)$$

After performing the integration over  $\psi_R$ ,  $\psi_R^\dagger$ ,  $\psi_L$  and  $\psi_L^\dagger$ , it becomes:

$$\exp(i\Gamma) = [\det(iG_L^{-1} + ig^2 U^2 \tilde{G}_R)], \quad (35)$$

where  $\Gamma$  is the quantum action that contains all quantum information of the system. Thus, the quantum action can be written as:

$$\begin{aligned} i\Gamma &= \ln[\det(iG_L^{-1} + g^2 U^2 \tilde{G}_R)] \\ &= \text{Tr}[\ln(iG_L^{-1} + ig^2 U^2 \tilde{G}_R)] \\ &= \text{Tr}[\ln(iG_L^{-1})(1 + g^2 U^2 G_L \tilde{G}_R)] \\ &= \text{Tr}[\ln(iG_L^{-1})] + \text{Tr}[\ln(1 + g^2 U^2 G_L \tilde{G}_R)]. \end{aligned} \quad (36)$$

Since it is very complicated to calculate  $\Gamma$  directly, a more general method is to expand  $\Gamma$  in powers of  $g$ . To the order of  $o(g^2)$ , the expression for  $\Gamma$  is:

$$i\Gamma = \text{Tr}[\ln(iG_L^{-1})] + \text{Tr}[\ln(1 + g^2 U^2 G_L \tilde{G}_R)] \approx \text{Tr}[\ln(iG_L^{-1})] + \text{Tr}(g^2 U^2 G_L \tilde{G}_R). \quad (37)$$

Here  $\text{Tr}[\ln(iG_L^{-1})]$  is an irrelevant constant that presents the vacuum energy of the Dirac field  $\{\psi_L(x), \psi_L^\dagger(x)\}$  in the absence of any interaction. Therefore, this irrelevant constant can be dropped, and then  $\Gamma$  can be expressed as:

$$\begin{aligned} \Gamma &= ig^2 \text{Tr}(U^2 G_L \tilde{G}_R) \\ &= ig^2 VT \int \frac{d^3 k}{(2\pi)^3} U^2(k^0, k^1, k^2) G_L(k^0, k^1, k^2) \tilde{G}_R(k^0, k^1, k^2) \\ &= ig^2 VT \int \frac{d^3 k}{(2\pi)^3} U^2(k^0, k^1, k^2) G_L(k^0, k^1, k^2) G_R(k^0 - vk^1, k^1, k^2) \\ &= ig^2 VT \int \frac{d^3 k}{(2\pi)^3} \frac{1}{(k^0)^2 - (k^1)^2 - (k^2)^2 + i\epsilon} \\ &\quad \times \frac{1}{(k^0)^2 - v_F^2(k^1)^2 - v_F^2(k^2)^2 - v_F^2 m^2 + i\epsilon} \\ &\quad \times \frac{1}{(k^0 - vk^1)^2 - v_F^2(k^1)^2 - v_F^2(k^2)^2 - v_F^2 m^2 + i\epsilon} \\ &\quad \times \text{tr} \left[ \begin{pmatrix} k^0 + v_F m & -v_F(k^1 - ik^2) \\ -v_F(k^1 + ik^2) & k^0 - v_F m \end{pmatrix} \begin{pmatrix} k^0 - vk^1 + v_F m & -v_F(k^1 - ik^2) \\ -v_F(k^1 + ik^2) & k^0 - vk^1 - v_F m \end{pmatrix} \right]. \end{aligned} \quad (38)$$

Here we derive the expression for the imaginary part of the quantum action and the dissipative force between the two plates of  $\text{Bi}_2\text{Se}_3$  surfaces. In our model, the R-plate is subject to an external force, rendering it an open system. Consequently, the vacuum state of the system becomes unstable, leading to particle excitations within the plates. Therefore, dissipation is associated with the imaginary part of the quantum action  $\Gamma$ . The quantum transition amplitude has a physical interpretation: its square represents the probability of the corresponding transition process. In this study, the probability of the vacuum-to-vacuum transition process is expressed as  $|Z|^2$ . For small  $\text{Im}\Gamma$ , this probability can be approximated perturbatively as:

$$|Z|^2 = |\exp(i\Gamma)|^2 = \exp(-2\text{Im}\Gamma) \approx 1 - 2\text{Im}\Gamma, \quad (39)$$

and the probability of particle production becomes:

$$\mathcal{P} = 1 - |Z|^2 = 2\text{Im}\Gamma. \quad (40)$$

To obtain the imaginary part of the quantum action, we first perform the integral over  $k^0$ , then the quantum action can be expressed as:

$$\Gamma = ig^2 VT \int \frac{d^3 k}{(2\pi)^3} f(k^0), \quad (41)$$

where

$$\begin{aligned}
f(k^0) = & \frac{1}{(k^0)^2 - (k^1)^2 - (k^2)^2 + i\epsilon} \\
& \times \frac{1}{(k^0)^2 - v_F^2(k^1)^2 - v_F^2(k^2)^2 - v_F^2m^2 + i\epsilon} \\
& \times \frac{1}{(k^0 - vk^1)^2 - v_F^2(k^1)^2 - v_F^2(k^2)^2 - v_F^2m^2 + i\epsilon} \\
& \times \text{tr} \left[ \begin{pmatrix} k^0 + v_F m & -v_F(k^1 - ik^2) \\ -v_F(k^1 + ik^2) & k^0 - v_F m \end{pmatrix} \begin{pmatrix} k^0 - vk^1 + v_F m & -v_F(k^1 - ik^2) \\ -v_F(k^1 + ik^2) & k^0 - vk^1 - v_F m \end{pmatrix} \right]. \tag{42}
\end{aligned}$$

In this case,  $f(k^0)$  has six single poles in the  $k^0$  complex plane, corresponding to on-shell particles, i.e., real particles. In this work, we study motion-dependent particle production, which requires selecting the poles based on the motion speed  $v$ , corresponding to the particles excited by the relative motion. These  $v$ -dependent poles of the function  $f(k^0)$  can be expressed as:

$$\Lambda_{\pm} = vk^1 \pm v_F \sqrt{(k^1)^2 + (k^2)^2 + m^2 - i\epsilon} \approx vk^1 \pm v_F \sqrt{(k^1)^2 + (k^2)^2 + m^2} \mp i\epsilon, \tag{43}$$

and the corresponding residues are given by:

$$\begin{aligned}
\text{Res}[f(k^0), \Lambda_{\pm}] = & \frac{1}{vk^1 \pm 2v_F \sqrt{(k^1)^2 + (k^2)^2 + m^2} \mp i\epsilon} \\
& \times \frac{\pm 1}{2v_F \sqrt{(k^1)^2 + (k^2)^2 + m^2} \mp i\epsilon} \times \frac{vk^1 - 2v_F \sqrt{(k^1)^2 + (k^2)^2 + m^2}}{vk^1} \\
& \times \frac{1}{(vk^1)[vk^1 \pm 2v_F \sqrt{(k^1)^2 + (k^2)^2 + m^2} + v_F^2[(k^1)^2 + (k^2)^2 + m^2] - (k^1)^2 - (k^2)^2 \mp i\epsilon]}. \tag{44}
\end{aligned}$$

Considering a contour formed by a semicircle with a very large radius in the bottom half of the complex plane and the real axis, we can complete the integral over  $k^0$  using the residue theorem<sup>22</sup>. Therefore, the quantum action can be written as:

$$\Gamma = g^2 V T \int \frac{dk^2}{2\pi} \int \frac{dk^1}{2\pi} \text{Res}[f(k^0), \Lambda_-]. \tag{45}$$

Both the contribution from the off-shell electrons (i.e., the vacuum fluctuation) and the on-shell electrons have been contained, so the quantum action can be written as:

$$\begin{aligned}
\Gamma = & g^2 V T \int \frac{dk^2}{2\pi} \int \frac{dk^1}{2\pi} \frac{1}{vk^1 - 2v_F \sqrt{(k^1)^2 + (k^2)^2 + m^2} + i\epsilon} \\
& \times \frac{-1}{2v_F \sqrt{(k^1)^2 + (k^2)^2 + m^2} + i\epsilon} \times \frac{vk^1 - 2v_F \sqrt{(k^1)^2 + (k^2)^2 + m^2}}{vk^1} \\
& \times \frac{1}{(vk^1)[vk^1 + 2v_F \sqrt{(k^1)^2 + (k^2)^2 + m^2} + v_F^2[(k^1)^2 + (k^2)^2 + m^2] - (k^1)^2 - (k^2)^2 + i\epsilon]}. \tag{46}
\end{aligned}$$

The imaginary part of  $\Gamma$  is:

$$\begin{aligned}
\text{Im}\Gamma = & g^2 V T \int \frac{dk^2}{2\pi} \int \frac{dk^1}{2\pi} \text{Im} \left( \frac{1}{vk^1 - 2v_F \sqrt{(k^1)^2 + (k^2)^2 + m^2} + i\epsilon} \right) \\
& \times \frac{-1}{2v_F \sqrt{(k^1)^2 + (k^2)^2 + m^2} + i\epsilon} \times \frac{vk^1 - 2v_F \sqrt{(k^1)^2 + (k^2)^2 + m^2}}{vk^1} \\
& \times \frac{1}{(vk^1)[vk^1 + 2v_F \sqrt{(k^1)^2 + (k^2)^2 + m^2} + v_F^2[(k^1)^2 + (k^2)^2 + m^2] - (k^1)^2 - (k^2)^2 + i\epsilon]}. \tag{47}
\end{aligned}$$

For any real function  $\frac{1}{a}$ , it has:

$$\lim_{\varepsilon \rightarrow 0} \frac{1}{a \pm i\varepsilon} = \mathbf{p.v.} \left( \frac{1}{a} \right) \mp i\pi\delta(a), \quad (48)$$

where **p.v.** means the principal value. This indicates that  $\text{Im} \left( \frac{1}{a+i\varepsilon} \right) = \pi\delta(a)$ , and then we can write:

$$\begin{aligned} \text{Im}\Gamma = & g^2 VT \int \frac{dk^2}{2\pi} \int \frac{dk^1}{2\pi} \delta[vk^1 - 2v_F \sqrt{(k^1)^2 + (k^2)^2 + m^2}] \\ & \times \frac{-1}{2v_F \sqrt{(k^1)^2 + (k^2)^2 + m^2} + i\varepsilon} \times \frac{vk^1 - 2v_F \sqrt{(k^1)^2 + (k^2)^2 + m^2}}{vk^1} \\ & \times \frac{1}{(vk^1)[vk^1 + 2v_F \sqrt{(k^1)^2 + (k^2)^2 + m^2}] + v_F^2[(k^1)^2 + (k^2)^2 + m^2] - (k^1)^2 - (k^2)^2 + i\varepsilon}. \end{aligned} \quad (49)$$

The imaginary part of  $\Gamma$  represents dissipation as well as the production of electrons from the initial vacuum. Relative motion causes energy transfer between electrons and introduces imaginary components in theoretical calculations. The energy of a single electron transforms as  $\omega'_k = \omega_k + vk^1$  under the Galilean boost of the coordinate system, where  $vk^1$  can be interpreted as the energy supplied to the system by the external force. From Eq. (49), it follows that both plates have an excited electron with energy  $vk^1$  due to the transformation. By the properties of the Dirac  $\delta$ -function, we know that:

$$\delta[vk^1 - 2v_F \sqrt{(k^1)^2 + (k^2)^2 + m^2}] = \frac{v}{v^2 - 4v_F^2} [\delta(k^1 - 2v_F \sqrt{\frac{(k^2)^2 + m^2}{v^2 - 4v_F^2}}) + \delta(k^1 + 2v_F \sqrt{\frac{(k^2)^2 + m^2}{v^2 - 4v_F^2}})]. \quad (50)$$

Thus, the imaginary part of  $\Gamma$ , after completing the integral over  $k^1$ , can be expressed as:

$$\text{Im}\Gamma = \frac{g^2 v_F V T}{4} (v^2 - 4v_F^2)^{\frac{3}{2}} \int \frac{dk^2}{2\pi} \frac{1}{\sqrt{v_F^2(k^2)^2 + v_F^2 m^2}} \frac{1}{(1 - 9v_F^2)v^2(k^2)^2 - (9v^2 - 4)v_F^2 m^2}. \quad (51)$$

Now we substitute the experimentally measured values of the Fermi velocity  $v_F$  into Eq. (51) to examine how  $\text{Im}\Gamma$  varies with  $v_F$ . Three representative Fermi velocities reported for  $\text{Bi}_2\text{Se}_3$  are considered. The earliest angle-resolved photoemission spectroscopy (ARPES) measurements of the surface-state dispersion yield  $v_F \approx 3 \times 10^5$  m/s<sup>39,40</sup>. A slightly larger value,  $v_F \approx 4.2 \times 10^5$  m/s, was obtained from ARPES measurements of the linear dispersion of the topological surface states  $E(k)$ , where the slope was determined using  $E = \hbar v_F k$ <sup>41-43</sup>. The third value,  $v_F \approx 2.2 \times 10^5$  m/s, was extracted from Shubnikov-de Haas (SdH) quantum oscillation data for pure  $\text{Bi}_2\text{Se}_3$ <sup>44</sup>. Figure 3 presents the numerical results of Eq. (51) for these three values of  $v_F$  with  $m = 1$  fixed, showing a threshold at the relative velocity  $v = 2v_F$ . This result indicates that dissipation occurs when  $v > 2v_F$ . The parameter  $m$ , which represents a controllable external magnetic field, has little influence on the overall trend of  $\text{Im}\Gamma$  as a function of  $v_F$  and only causes a rescaling of the coordinate axes. We give the test of different values of  $m$  for Eq. (51) in Appendix A. The dissipation occurring in the system refers to an energy transfer process, since it is an external force acting on the R-plate. As the relative motion progresses, energy is continuously pumped into the system. This energy excites electrons at the interface between both plates. Thus, the equation of energy transfer can be written as:

$$\frac{E_{\text{pump}}}{VT} = \frac{E_{\text{diss}}}{VT}, \quad (52)$$

which indicates the power of energy pumped into the system ( $E_{\text{pump}}$ ) equals the dissipation power ( $E_{\text{diss}}$ ). To maintain the relative motion between the two plates, a continuous external force must be applied to the R-plate to counteract the frictional force between the plates. Only in this way can the external source resist friction and maintain uniform relative motion. The dissipation energy from the excitation of electrons can be expressed as:

$$E_{\text{diss}} = g^2 V T \text{Im} \int \frac{d^3k}{(2\pi)^3} i f(k^0) |k^0|, \quad (53)$$

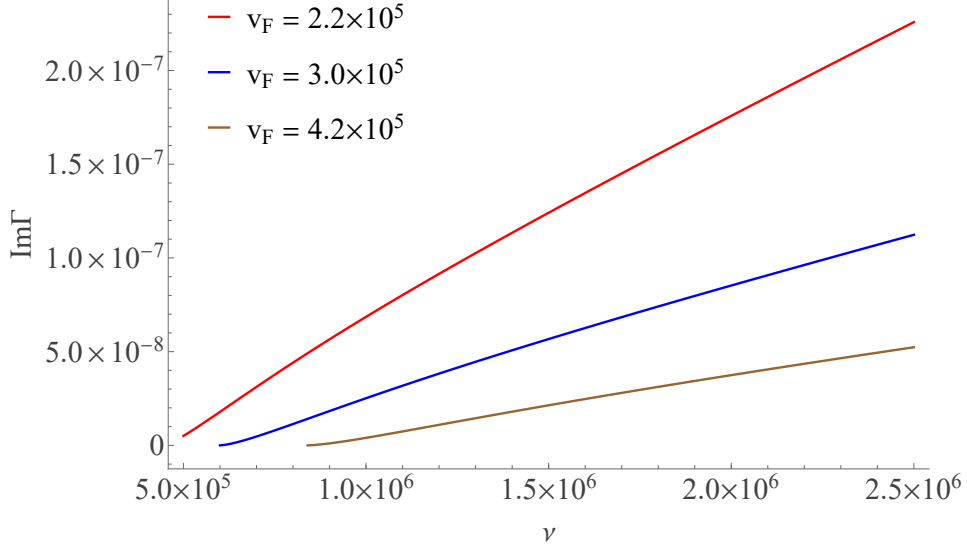


**Figure 3.** The imaginary part of quantum action as a function of  $v$ , for the case  $v_F = 3 \times 10^5, 4.2 \times 10^5$  and  $2.2 \times 10^5$ , with  $m = 1$ , in units of  $g^2 TV$ .

and the dissipation power can be written as:

$$\frac{E_{\text{diss}}}{VT} = F_{\text{diss}} v. \quad (54)$$

Thus, we can achieve the dissipative force as:

$$F_{\text{diss}} = \frac{1}{v} g^2 \text{Im} \int \frac{d^3 k}{(2\pi)^3} i f(k^0) |k^0|. \quad (55)$$

The explicit expression of the dissipative force can be obtained from Eq. (42) as:

$$F_{\text{diss}} = \frac{3g^2 v_F}{4v} (v^2 - 4v_F^2)^{\frac{3}{2}} \int \frac{dk^2}{2\pi} \frac{1}{\sqrt{v_F^2(k^2)^2 + v_F^2 m^2}} \frac{1}{(1 - 9v_F^2)v^2(k^2)^2 - (9v^2 - 4)v_F^2 m^2}. \quad (56)$$

Similarly, we use the three values of  $V_F$  for  $\text{Im}\Gamma$  to demonstrate the numerical result of  $F_{\text{diss}}$  with  $m = 1$  in Fig. 4. We can see that it is a threshold of the relative velocity  $v = 2v_F$ , like the  $v$ -dependence of  $\text{Im}\Gamma$  in Fig. 3. The difference is, the in Fig. 4 the curve of  $F_{\text{diss}}$  shows linear behaviors, and the slope of the  $v - F_{\text{diss}}$  curves give linear friction coefficient at zero temperature. To deeply understand the existence of thresholds for  $\text{Im}\Gamma$  and  $F_{\text{diss}}$ , we can focus on the Dirac  $\delta$ -function  $\delta(vk^1 - 2v_F \sqrt{(k^1)^2 + (k^2)^2 + m^2})$ , the resonance to the external force acting on the Dirac fields living in the plates. This resonance implies production of the on-shell electrons, and the most easily excited electrons are the massless ones, i.e.,  $2v_F \sqrt{(k^1)^2 + (k^2)^2}$ .

Our results indicate that under relative motion, both the imaginary part of the quantum action  $\text{Im}\Gamma$  and the dissipative force  $F_{\text{diss}}$  exhibit a distinct velocity threshold behavior. When the relative velocity  $v$  exceeds twice the Fermi velocity  $2v_F$ , the system undergoes pronounced quantum dissipation. This threshold provides a clear criterion for experimentally detecting and controlling energy dissipation between  $\text{Bi}_2\text{Se}_3$  interfaces. Moreover, a linear relationship between the dissipative force and the relative velocity is observed, implying the existence of a linear friction coefficient at zero temperature. This finding offers new insights into the energy-loss mechanisms of  $\text{Bi}_2\text{Se}_3$  films under sliding contact or nonequilibrium transport. Overall, these results deepen the understanding of quantum dissipation in topological insulators and provide a theoretical foundation for designing low-dissipation nanodevices and developing quantum interface control strategies based on  $\text{Bi}_2\text{Se}_3$ .

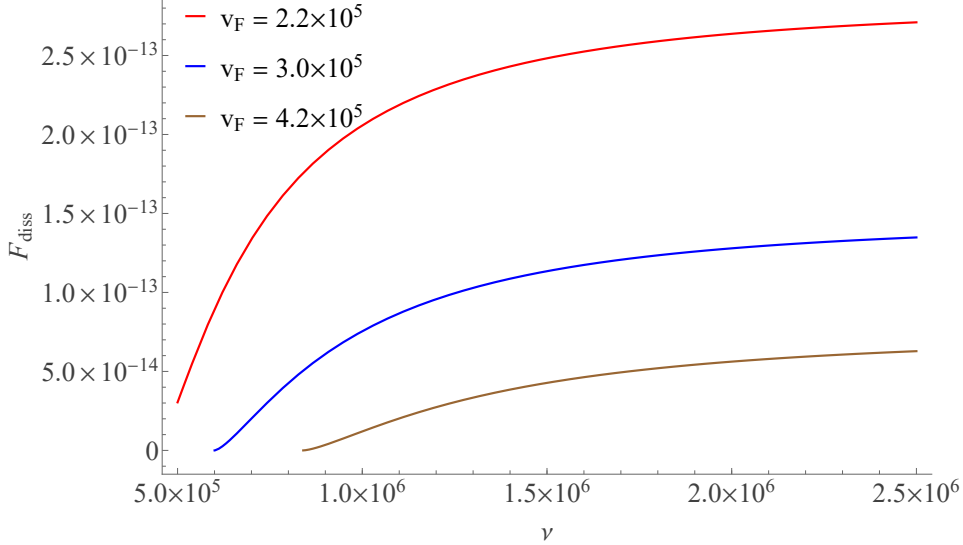


**Figure 4.** The dissipative force as a function of  $v$ , for the case  $v_F = 3 \times 10^5, 4.2 \times 10^5$  and  $2.2 \times 10^5$ , with  $m = 1$ , in units of  $g^2 TV$ .

## 7 Conclusion

In this paper, we studied the excitation and quantum dissipation of two  $\text{Bi}_2\text{Se}_3$  surfaces induced by the internal relative motion of two parallel metallic plates. The degrees of freedom (DOFs) of the electrons in both plates were modeled using the 1+2 dimensional Dirac field, and a nonlocal potential was chosen to describe the interaction between L-electrons and R-electrons. The internal relative motion was introduced via a Galilean boost.

Specifically, by assuming the L-plate is stationary while the R-plate moves along the interface, we derived the effective action of the L-electrons by integrating out the R-electrons and then calculated the vacuum occupation number  $n_L(\mathbf{k})$  in momentum space perturbatively. According to the numerical results,  $n_L(\mathbf{k})$  is isotropic with respect to momentum for  $v = 0$  and becomes anisotropic for nonzero  $v$ , as expected. The perturbative approximation applied here operates in a nonequilibrium steady-state (NESS) regime, where the system remains close to the initial vacuum state.

Subsequently, we derived the expression for the imaginary part of the quantum action  $\text{Im}\Gamma$  due to the relative motion and calculated the dissipative force  $F_{\text{diss}}$  between the two plates. The numerical results show that both  $\text{Im}\Gamma$  and  $F_{\text{diss}}$  exhibit a threshold and are positively correlated with  $v$ . Notably, the dependence of  $F_{\text{diss}}$  on  $v$  follows a linear relationship, leading to a linear friction coefficient at zero temperature. The dissipation velocity threshold ( $v > 2v_F$ ) and the linear friction relationship revealed in this study provide a solid theoretical foundation for experimentally detecting and controlling quantum energy dissipation at  $\text{Bi}_2\text{Se}_3$  interfaces. These findings are crucial for understanding the nonequilibrium transport behavior of this topological insulator in nanoscale systems and for guiding the design of low-dissipation quantum devices.

In this study, the dissipation rate threshold ( $v > 2v_F$ ) and the linear friction relationship revealed by the theoretical model of  $\text{Bi}_2\text{Se}_3$  provide a solid theoretical foundation for experimentally detecting and controlling quantum energy dissipation between its topological interfaces. It is worth highlighting that we employed a specific physical motivation for the nonlocal interaction  $U$  in our calculations. The coupling between the two plates is assumed to be s-d coupling, which originates from fundamental electromagnetic interactions and is inherently nonlocal. Since condensed matter systems often feature complex and novel excitations, this method could also be applied to other systems beyond electrons. However, for strongly correlated systems without a well-defined quasi-particle picture, non-perturbative approaches to quantum dissipation are also worth exploring.

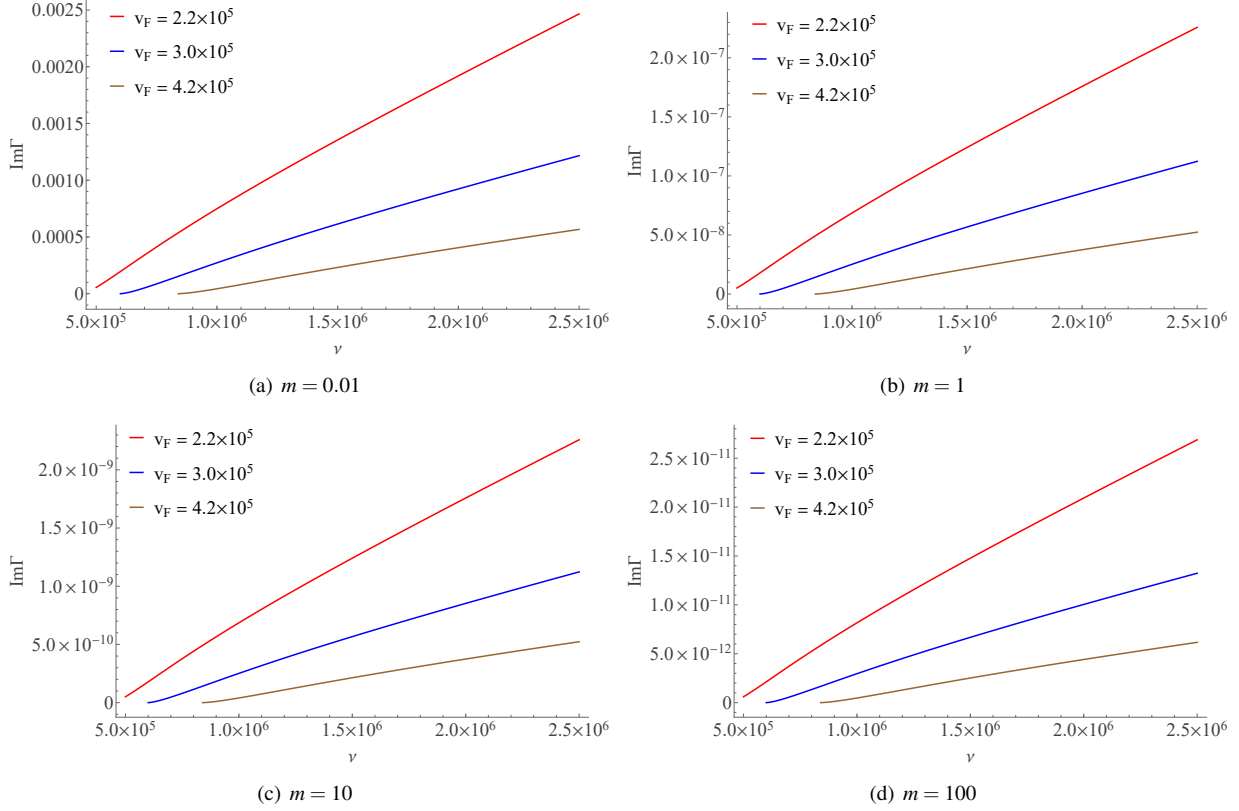


**Figure 5.** The imaginary part of quantum action as a function of  $\nu$ , for the case  $v_F = 3 \times 10^5, 4.2 \times 10^5$  and  $2.2 \times 10^5$ , in units of  $g^2 TV$ , with (a)  $m = 0.01$ , (b)  $m = 1$ , (c)  $m = 10$  and (d)  $m = 100$ .

## A The impact of different values $m$ on $\text{Im}\Gamma$ and $F_{\text{diss}}$

Here we discuss the changes in the results of  $\text{Im}\Gamma$  and  $F_{\text{diss}}$  under different values of  $m$ . While keeping the value of  $v_F$  unchanged and substituting  $m = 0.01$  into  $\text{Im}\Gamma$  (Eq. (51)), Fig. 5 shows that its magnitude decreases along the y-axis as  $m$  increases, while the shapes of the three curves remain unchanged. The similar behavior is observed for  $F_{\text{diss}}$  (Eq. (56)) in Fig. 6, indicating that in our model, variations in the external magnetic moment affect only the magnitudes of  $\text{Im}\Gamma$  and  $F_{\text{diss}}$ .

## Acknowledgement

We gratefully acknowledge Qiang Sun for valuable discussions. This research was supported by Yunnan Fundamental Research Projects (Grant No. 202401AU070125), the Special Basic Cooperative Research Programs of Yunnan Provincial Undergraduate Universities' Association (Grant No. 202301BA070001-114), Yunnan Provincial Department of Education Science Research Fund Project (No. 2025J0942), 2025 Self-funded Science and Technology Projects of Chuxiong Prefecture (Grant No. cxzc2025004, cxzc2025008), Chuxiong Normal University Doctoral Research Initiation Fund Project (No. BSQD2407, BSQD2507), Yunnan Provincial Department of Education Science Research Fund Project (No. 2025J0942) and Dongying Science Development Fund Project (No. DJB2023015).

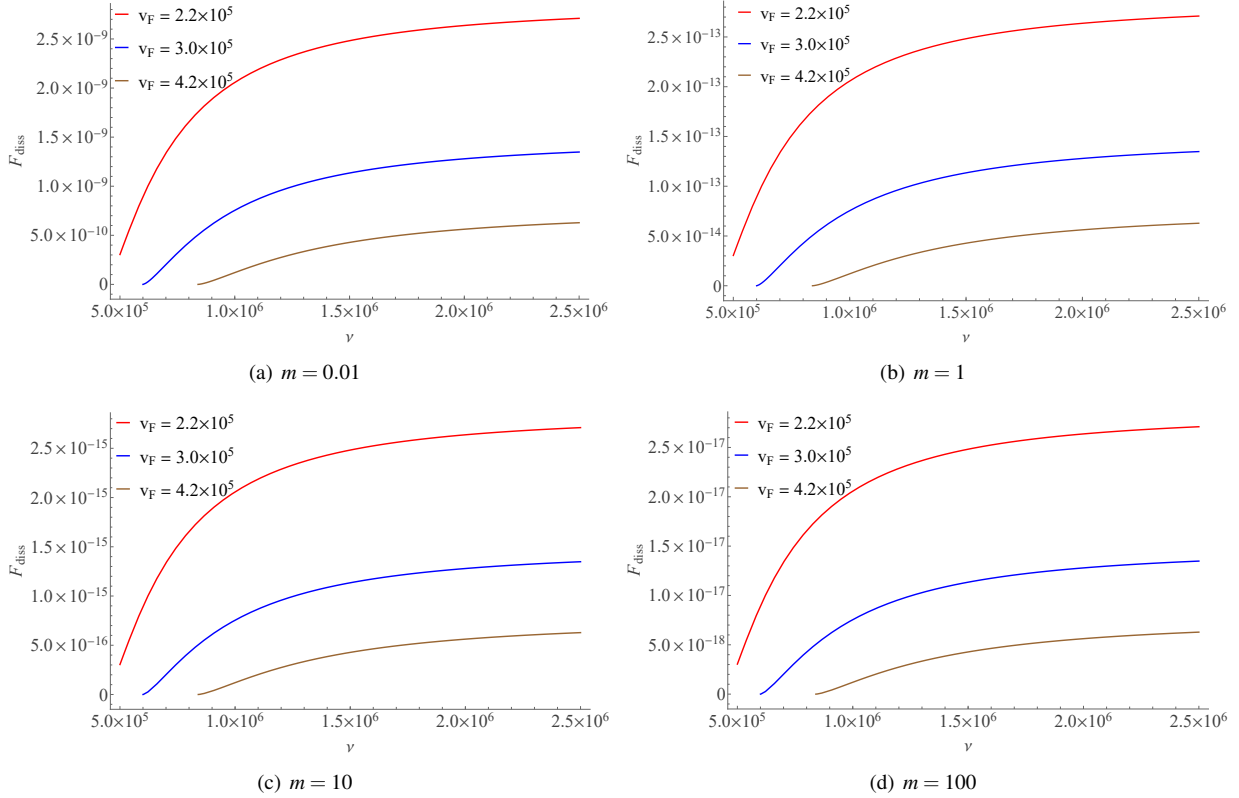


**Figure 6.** The dissipative force as a function of  $v$ , for the case  $v_F = 3 \times 10^5, 4.2 \times 10^5$  and  $2.2 \times 10^5$ , in units of  $g^2 TV$ , with (a)  $m = 0.01$ , (b)  $m = 1$ , (c)  $m = 10$  and (d)  $m = 100$ .

## References

1. Hasan, M. Z. & Kane, C. L. Colloquium: Topological insulators. *Rev. Mod. Phys.* **82**, 3045–3067 (2010).
2. Qi, X.-L. & Zhang, S.-C. Topological insulators and superconductors. *Rev. Mod. Phys.* **83**, 1057–1110 (2011).
3. Zhang, D. *et al.* Superconducting proximity effect and possible evidence for pearl vortices in a candidate topological insulator. *Phys. Rev. B* **84**, 165120, DOI: [10.1103/PhysRevB.84.165120](https://doi.org/10.1103/PhysRevB.84.165120) (2011).
4. Xia, Y. *et al.* Observation of a large-gap topological-insulator class with a single dirac cone on the surface. *Nat. Phys.* **5**, 398–402 (2009).
5. Ghaemi, P., Mong, R. S. K. & Moore, J. E. In-plane transport and enhanced thermoelectric performance in thin films of the topological insulators  $\text{Bi}_2\text{Te}_3$  and  $\text{Bi}_2\text{Se}_3$ . *Phys. Rev. Lett.* **105**, 166603, DOI: [10.1103/PhysRevLett.105.166603](https://doi.org/10.1103/PhysRevLett.105.166603) (2010).
6. Jin, H., Song, J.-H. & Freeman, A. J. Dirac cone engineering in  $\text{Bi}_2\text{Se}_3$  thin films. *Phys. Rev. B* **83**, 125319, DOI: [10.1103/PhysRevB.83.125319](https://doi.org/10.1103/PhysRevB.83.125319) (2011).
7. Young, S. M. *et al.* Theoretical investigation of the evolution of the topological phase of  $\text{Bi}_2\text{Se}_3$  under mechanical strain. *Phys. Rev. B* **84**, 085106, DOI: [10.1103/PhysRevB.84.085106](https://doi.org/10.1103/PhysRevB.84.085106) (2011).
8. Xu, R. & Yan, Y. Theory of open quantum systems. *The J. Chem. Phys.* **116**, 9196–9206, DOI: [10.1063/1.1474579](https://doi.org/10.1063/1.1474579) (2002).
9. Joichi, I., Matsumoto, S. & Yoshimura, M. Quantum Dissipation in Open Harmonic Systems:  $\hat{A}$ -Operator Solution and Application to Decay Process. *Prog. Theor. Phys.* **98**, 9–28, DOI: [10.1143/PTP.98.9](https://doi.org/10.1143/PTP.98.9) (1997).
10. The theory of a general quantum system interacting with a linear dissipative system. *Annals Phys.* **281**, 547–607, DOI: <https://doi.org/10.1006/aphy.2000.6017> (2000).
11. Zhang, L. & Wang, C. Quantum markov semigroup for open quantum system interacting with quantum bernoulli noises. *Rev. Math. Phys.* **35**, 2350015, DOI: [10.1142/S0129055X23500150](https://doi.org/10.1142/S0129055X23500150) (2023).
12. Xu, R.-X. & Yan, Y. Dynamics of quantum dissipation systems interacting with bosonic canonical bath: Hierarchical equations of motion approach. *Phys. Rev. E* **75**, 031107, DOI: [10.1103/PhysRevE.75.031107](https://doi.org/10.1103/PhysRevE.75.031107) (2007).
13. Jin, J. *et al.* Dynamics of quantum dissipation systems interacting with fermion and boson grand canonical bath ensembles: Hierarchical equations of motion approach. *The J. Chem. Phys.* **126**, 134113, DOI: [10.1063/1.2713104](https://doi.org/10.1063/1.2713104) (2007).
14. Degrande, C. *et al.* Effective field theory: A modern approach to anomalous couplings. *Annals Phys.* **335**, 21–32, DOI: <https://doi.org/10.1016/j.aop.2013.04.016> (2013).
15. Wen, X.-G. *Quantum Field Theory of Many-Body Systems: From the Origin of Sound to an Origin of Light and Electrons* (Oxford University Press, 2007).
16. Vasiliev, A. N. *Functional methods in quantum field theory and statistical physics* (CRC Press, 1998).
17. Berera, A., Gleiser, M. & Ramos, R. O. Strong dissipative behavior in quantum field theory. *Phys. Rev. D* **58**, 123508, DOI: [10.1103/PhysRevD.58.123508](https://doi.org/10.1103/PhysRevD.58.123508) (1998).
18. Peskin, M. E., Schroeder, D. V. & Martinec, E. An Introduction to Quantum Field Theory. *Phys. Today* **49**, 69–72, DOI: [10.1063/1.2807734](https://doi.org/10.1063/1.2807734) (1996).
19. Jentschura, U. D. Friction effects in atom-surface interactions. In *APS Division of Atomic, Molecular and Optical Physics Meeting Abstracts*, vol. 2016, B5–010 (2016).
20. Wang, Y. & Jia, Y. Quantum dissipation and friction attributed to plasmons. *Mod. Phys. Lett. B* **36**, 2150589, DOI: [10.1142/S0217984921505898](https://doi.org/10.1142/S0217984921505898) (2022).
21. Dodonov, A. V. Dynamical casimir effect via four- and five-photon transitions using a strongly detuned atom. *Phys. Rev. A* **100**, 032510, DOI: [10.1103/PhysRevA.100.032510](https://doi.org/10.1103/PhysRevA.100.032510) (2019).
22. Fosco, C. D., Lombardo, F. C. & Mazzitelli, F. D. Quantum dissipative effects in moving imperfect mirrors: Sidewise and normal motions. *Phys. Rev. D* **84**, 025011, DOI: [10.1103/PhysRevD.84.025011](https://doi.org/10.1103/PhysRevD.84.025011) (2011).

23. *The Phonon Dissipation Mode in Nanofriction*, vol. Volume 10: Micro- and Nano-Systems Engineering and Packaging of ASME International Mechanical Engineering Congress and Exposition. DOI: [10.1115/IMECE2016-66402](https://doi.org/10.1115/IMECE2016-66402).
24. Magiera, M. P., Wolf, D. E., Brendel, L. & Nowak, U. Magnetic friction and the role of temperature. *IEEE Transactions on Magn.* **45**, 3938–3941, DOI: [10.1109/TMAG.2009.2023623](https://doi.org/10.1109/TMAG.2009.2023623) (2009).
25. Persson, B. Electronic friction on a superconductor surface. *Solid State Commun.* **115**, 145–148, DOI: [https://doi.org/10.1016/S0038-1098\(00\)00151-4](https://doi.org/10.1016/S0038-1098(00)00151-4) (2000).
26. Dou, W. & Subotnik, J. E. Electronic friction near metal surfaces: A case where molecule-metal couplings depend on nuclear coordinates. *The J. Chem. Phys.* **146**, 092304, DOI: [10.1063/1.4965823](https://doi.org/10.1063/1.4965823) (2016).
27. Fosco, C. D., Lombardo, F. C. & Mazzitelli, F. D. Quantum dissipative effects in moving mirrors: A functional approach. *Phys. Rev. D* **76**, 085007, DOI: [10.1103/PhysRevD.76.085007](https://doi.org/10.1103/PhysRevD.76.085007) (2007).
28. Viotti, L., Belén Fariás, M., Villar, P. I. & Lombardo, F. C. Thermal corrections to quantum friction and decoherence: A closed-time-path approach to atom-surface interaction. *Phys. Rev. D* **99**, 105005, DOI: [10.1103/PhysRevD.99.105005](https://doi.org/10.1103/PhysRevD.99.105005) (2019).
29. Farias, M. B., Fosco, C. D., Lombardo, F. C. & Mazzitelli, F. D. Quantum friction between graphene sheets. *Phys. Rev. D* **95**, 065012, DOI: [10.1103/PhysRevD.95.065012](https://doi.org/10.1103/PhysRevD.95.065012) (2017).
30. Fariás, M. B. & Lombardo, F. C. Dissipation and decoherence effects on a moving particle in front of a dielectric plate. *Phys. Rev. D* **93**, 065035, DOI: [10.1103/PhysRevD.93.065035](https://doi.org/10.1103/PhysRevD.93.065035) (2016).
31. Wang, Y., Zhang, R. & Liu, F. The magnon mediated plasmon friction: a functional integral approach. *arXiv:2408.01405* (2024). [arXiv:2408.01405](https://arxiv.org/abs/2408.01405).
32. Ando, Y. Topological insulator materials. *J. Phys. Soc. Jpn.* **82**, 102001, DOI: [10.7566/JPSJ.82.102001](https://doi.org/10.7566/JPSJ.82.102001) (2013).
33. Golkar, S., Roberts, M. & Dam, S. Effective field theory of relativistic quantum hall systems. *J. High Energy Phys.* **2014**, 138, DOI: [10.1007/JHEP12%282014%29138](https://doi.org/10.1007/JHEP12%282014%29138) (2014).
34. Dou, W., Miao, G. & Subotnik, J. E. Born-oppenheimer dynamics, electronic friction, and the inclusion of electron-electron interactions. *Phys. Rev. Lett.* **119**, 046001, DOI: [10.1103/PhysRevLett.119.046001](https://doi.org/10.1103/PhysRevLett.119.046001) (2017).
35. Weinberg, S. & Greenberg, O. W. The Quantum Theory of Fields, Vol. 1: Foundations. *Phys. Today* **48**, 78–78, DOI: [10.1063/1.2808256](https://doi.org/10.1063/1.2808256) (1995).
36. Hollik, W. Quantum Field Theory and the Standard Model. *Phys. Today* **67**, 57–58, DOI: [10.1063/PT.3.2624](https://doi.org/10.1063/PT.3.2624) (2014).
37. Kim, S. P. & Page, D. N. Schwinger pair production in electric and magnetic fields. *Phys. Rev. D* **73**, 065020, DOI: [10.1103/PhysRevD.73.065020](https://doi.org/10.1103/PhysRevD.73.065020) (2006).
38. Olesen, P. On vacuum instability in quantum field theory. *Phys. Lett. B* **73**, 327–329, DOI: [https://doi.org/10.1016/0370-2693\(78\)90526-9](https://doi.org/10.1016/0370-2693(78)90526-9) (1978).
39. Cha, J. J. *et al.* Effects of magnetic doping on weak antilocalization in narrow  $\text{Bi}_2\text{Se}_3$  nanoribbons. *Nano Lett.* **12**, 4355–4359, DOI: [10.1021/nl3021472](https://doi.org/10.1021/nl3021472) (2012). PMID: 22830578.
40. Kim, D., Syers, P., Butch, N. P., Paglione, J. & Fuhrer, M. S. Coherent topological transport on the surface of  $\text{Bi}_2\text{Se}_3$ . *Nat. communications* **4**, 2040 (2013).
41. Checkelsky, J. G., Hor, Y. S., Cava, R. J. & Ong, N. Bulk band gap and surface state conduction observed in voltage-tuned crystals<? format?> of the topological insulator  $\text{Bi}_2\text{Se}_3$ . *Phys. review letters* **106**, 196801 (2011).
42. Zhang, Y. *et al.* Crossover of the three-dimensional topological insulator  $\text{Bi}_2\text{Se}_3$  to the two-dimensional limit. *Nat. Phys.* **6**, 584–588 (2010).
43. Galletti, L. *et al.* Influence of topological edge states on the properties of  $\text{Al}/\text{Bi}_2\text{Se}_3/\text{Al}$  hybrid josephson devices. *Phys. Rev. B* **89**, 134512, DOI: [10.1103/PhysRevB.89.134512](https://doi.org/10.1103/PhysRevB.89.134512) (2014).
44. Chen, L. *et al.* Magnetotransport and berry phase tuning in gd-doped  $\text{Bi}_2\text{Se}_3$  topological insulator single crystals. *Phys. Rev. Mater.* **6**, 054202, DOI: [10.1103/PhysRevMaterials.6.054202](https://doi.org/10.1103/PhysRevMaterials.6.054202) (2022).